

Evidence for a Finite-Temperature Spin Glass Transition in a Diluted Dipolar Heisenberg Model in Three Dimensions

Pawel Stasiak

Department of Physics and Astronomy, University of Waterloo, Waterloo, Ontario, N2L-3G1 Canada

Michel J. P. Gingras

*Department of Physics and Astronomy, University of Waterloo, Waterloo, Ontario, N2L-3G1 Canada and
Canadian Institute for Advanced Research, 180 Dundas St. W., Toronto, Ontario, M5G 1Z8, Canada*

(Dated: October 29, 2018)

By means of parallel tempering Monte Carlo simulations we find strong evidence for a finite-temperature spin-glass transition in a system of diluted classical Heisenberg dipoles randomly placed on the sites of a simple cubic lattice. We perform a finite-size scaling analysis of the spin-glass susceptibility, χ_{SG} , and spin-glass correlation length, ξ_L . For the available system sizes that can be successfully equilibrated, the crossing of ξ_L/L versus temperature is strongly affected by corrections to scaling and possibly by a short-length scale ferromagnetic spin blocking. Similarly to many studies of different three dimensional spin-glass systems, we do not find a crossing of the spin glass order parameter Binder ratio.

I. INTRODUCTION

Our most formal current theoretical understanding of the spin-glass (SG) phase is based on the replica symmetry breaking (RSB) picture set by the Parisi solution^{1,2} of the infinite-dimensional Sherrington-Kirkpatrick model.³ As the upper critical dimension (UCD) of SG models is large ($d_{UCD}=6$),⁴ such mean-field description is likely to be unsuitable to understand the physics of real materials exhibiting glassy behavior. An alternative description of the SG phase in finite dimension is given by the phenomenological droplet picture,⁵ which has been found to possibly characterize better three dimensional (3D) SG.⁶ However, it remains an open debate what is the proper theory describing SG systems in real (finite) dimensions. Most of our knowledge about the properties of 3D SG models has been assembled thanks to years of extensive numerical simulations. Unfortunately, the slow relaxation characterizing spin glass systems makes the numerical studies very difficult. Furthermore, the largest fraction of the numerical work has so far concentrated on the Edwards-Anderson (EA) model⁷ of n -component spins interacting via nearest-neighbor random exchange interaction, J_{ij} , where both ferromagnetic or antiferromagnetic couplings are present. The cases $n=1$ and $n=3$ refer to Ising and Heisenberg SG, respectively. The probability distribution of the random bonds, $P(J_{ij})$, is usually taken to be Gaussian or bimodal.^{4,8}

A great part of the numerical studies of SG models has been devoted to the minimal EA model, the one-component Ising SG. Due to severe technical difficulties, only very limited range of system sizes was accessible in the early simulations, while scaling corrections in SG systems are large. As a result, the existence of a finite temperature SG transition in 3D Ising SG model had remained under debate for a long time.^{9,10,11,12,13,14} The early MC studies strongly supported the finite-temperature SG transition, but zero-temperature tran-

sition could not be definitely ruled out.^{9,10,15} Only quite recently, in the course of large-scale Monte Carlo studies, has the existence of a thermodynamic phase transition in the Ising case been seemingly firmly established¹¹ and, perhaps most satisfactorily, universality among systems with different bond distributions been confirmed.^{12,13}

The case of the Heisenberg SG still remains somewhat more controversial than of the Ising SG. Originally, it was believed that the lower critical dimension (LCD) for the Heisenberg SG is $d_{LCD} \geq 3$,¹⁶ and that the small anisotropies present in the real system are responsible for the SG behavior observed in experiments.^{16,17} While compelling, this suggestion has some difficulties since no crossover from Heisenberg to Ising SG universality class caused by a weak anisotropy has ever been observed in experiments.^{18,19} It was suggested that in the Heisenberg EA SG, a finite-temperature transition occurs in the chiral sector^{18,19} while a SG transition in the spin sector occurs at zero temperature.^{19,20,21} The chirality is a multi-spin variable representing the handedness of the noncolinear or noncoplanar spin structures.^{18,19} It has been proposed that the SG phase in Heisenberg SG materials is caused by a spin-chirality coupling induced by small anisotropies.¹⁹ Later simulations indicated the existence of a nonzero-temperature SG transition.^{22,23} The most recent work on the 3D Heisenberg SG suggests that the SG transition may be decoupled from the chiral glass (CG) transition, occurring at slightly higher temperature,^{24,25} or that a common transition temperature may exist.²⁶ In two dimensions, recent defect-wall renormalization group calculations suggest that both the SG and CG transitions occur at zero temperature, but that the two transitions are decoupled.^{27,28,29}

On the experimental side there exist some SG materials with a strong Ising-like uniaxial anisotropy, but the majority of experimental SG studies focus on nearly isotropic, Heisenberg-like systems. A well studied Ising SG material is $\text{Fe}_{0.5}\text{Mn}_{0.5}\text{TiO}_3$,^{30,31} as other examples of an Ising SG more recently found, $\text{Eu}_{0.5}\text{Ba}_{0.5}\text{MnO}_3$.³²

and $\text{Cu}_{0.5}\text{Co}_{0.5}\text{Cl}_2\text{-FeCl}_3$ ^{33,34} can be mentioned. Considering $\text{Fe}_{0.5}\text{Mn}_{0.5}\text{TiO}_3$,^{30,31} the leading coupling is a nearest-neighbor exchange, and the compounds, FeTiO_3 and MnTiO_3 , are antiferromagnets. In both cases, the nearest-neighbor exchange interactions within the hexagonal layers is antiferromagnetic. The magnitude of the intralayer coupling is substantially larger than the interlayer coupling. The SG nature of the mixture, $\text{Fe}_{0.5}\text{Mn}_{0.5}\text{TiO}_3$, originates from the fact that the coupling between the layers is ferromagnetic in FeTiO_3 but antiferromagnetic in MnTiO_3 ;³⁰ hence, in the mixture, random frustration occurs. For the Heisenberg case, some short-range SG compounds are also available, for example insulating $\text{Eu}_x\text{Sr}_{1-x}\text{S}$.^{4,35} In the Eu-rich case, this material is a ferromagnet; the nearest-neighbor exchange interaction between Eu^{2+} ions is ferromagnetic and the next-nearest-neighbor exchange is weaker and antiferromagnetic.^{4,36} When magnetic Eu is randomly substituted with nonmagnetic Sr, a random frustration of the ferromagnetic and antiferromagnetic bonds arises. But the most often studied SG are nearly isotropic (Heisenberg) metallic systems interacting via a long-range Ruderman-Kittel-Kasuya-Yoshida (RKKY) interaction between localized magnetic moments mediated by conduction electrons. In this category, the classical systems are alloys of noble metals such as Ag, Au, Cu or Pt, doped with a transition metal, such as Fe or Mn, often labeled as canonical SGs. In the large r limit, where r is the distance separating the magnetic moments, the RKKY interaction varies with r as $\cos(2k_F r)/r^3$, where k_F is the Fermi wavevector.

Another class of SG materials consists of spatially disordered magnetic dipoles. The dipolar interaction has either ferromagnetic or antiferromagnetic character depending on the relative position of the interacting dipoles. In the presence of positional disorder, this gives rise to random frustration and a SG phase at low temperature and sufficiently high level of disorder is expected.³⁷ A number of dipolar Ising SG materials have been identified and related models have been studied numerically. With the aim of modeling nanosized magnetic particles dispersed in a frozen nonmagnetic solvent,⁴⁰ systems of Ising dipoles on fully occupied⁴¹ and diluted⁴² (with $x=35\%$ and $x=50\%$ occupancy) simple cubic (SC) lattice with randomly oriented easy axes have been simulated. In three dimensions, a spin-glass transition has been identified, both in the diluted⁴² and undiluted case.⁴¹ A well known physical realization of a diluted dipolar Ising model and dipolar SG is $\text{LiHo}_x\text{Y}_{1-x}\text{F}_4$.^{43,44,45,46} Early on, some authors suggested the existence of an exotic anti-glass phase at very low concentration, x ,^{43,47,48} or questioned the existence of SG transition in $\text{LiHo}_x\text{Y}_{1-x}\text{F}_4$ altogether.^{49,50} As well, early numerical studies of diluted Ising dipoles on SC lattice⁵¹ and for a lattice geometry corresponding to $\text{LiHo}_x\text{Y}_{1-x}\text{F}_4$ ⁵² did not find a spin-glass transition in diluted dipolar Ising systems.^{51,52} A more recent work, however, reports a spin-glass phase in a model approx-

imating $\text{LiHo}_x\text{Y}_{1-x}\text{F}_4$.⁴⁶ As in previous work,⁵² crossing of the spin-glass Binder ratio plots was not found in Ref. [46], but a finite-size scaling of the spin-glass correlation length provided a compelling evidence for a thermodynamical phase transition.⁴⁶ Apparently, the corrections to scaling are large for the sizes of dipolar systems studied, being very pronounced in the Binder ratio while the SG correlation length is somewhat less affected.⁴⁶ Very recent MC simulations of a site-diluted SC lattice of Ising spins coupled via a long-range dipolar interactions also found a finite-temperature spin-glass transition, but with different value of the correlation length exponent $\nu=0.95$,⁵³ compared with $\nu=1.3$ reported in Ref. [46].

The case of dipolar Heisenberg SG is an obvious extension of the SG phenomenology reviewed above. In the presence of spatial disorder, the off-diagonal terms in the dipolar interaction destroy the rotational symmetry of the ground state. Thus, the dipolar Heisenberg SG is expected to be in the Ising universality class.^{17,54,55} In this context, it would be interesting to study a three component ($n=3$, Heisenberg) SG system where anisotropic long-range interactions, i.e. dipolar interactions, dominate. Finding in such system critical exponents that are consistent with the exponents of Ising SG universality class would further confirm universality in spin glasses and boost our confidence in our largely numerically-based understanding of real spin glass systems.

Experimentally, a diluted dipolar SG can be realized by sufficiently diluting magnetic dipoles with a nonmagnetic substituent, to the point that a short-range exchange interaction becomes insignificant, and long-range dipolar interaction dominates. The best candidate materials are compounds containing rare earth magnetic ions, as due to the screening of the partially filled $4f$ shell by outer shells, the exchange interaction is relatively weak among rare earths, while their magnetic moments can be large.

It was mentioned above that $\text{Eu}_x\text{Sr}_{1-x}\text{S}$, at concentration $x \simeq 0.5$, is an example of a short-range Heisenberg SG, where the SG freezing is driven by the frustrated nearest-neighbor and next-nearest-neighbor exchange interactions. The $4f$ electrons of the rare earth Eu^{2+} ion give an $^8S_{7/2}$ ground state with a sizable magnetic moment of $7\mu_B$.³⁶ Below the percolation threshold, i.e. $x_c = 0.136$ for the face centered cubic lattice (FCC) with first- and second-nearest-neighbor interactions,⁵⁶ the existence of a dipolar SG in $\text{Eu}_x\text{Sr}_{1-x}\text{S}$ was suggested.⁵⁷ To explain the two maxima in the ac susceptibility, at temperatures of order of 100 mK and 10 mK, an interplay of dipolar freezing and blocking of small clusters was proposed.⁵⁷ But the authors of subsequent studies⁵⁸ suggested that the features in the ac susceptibility of $\text{Eu}_x\text{Sr}_{1-x}\text{S}$ at concentration $0.05 < x < 0.13$ should be interpreted as a spin blocking and not a dipolar SG freezing. Nevertheless, it was also proposed that maybe at lower concentration, x , a dipolar SG freezing in this material could be studied.⁵⁸ It should be reminded that the existence of a dipolar SG at high dilution in $\text{LiHo}_x\text{Y}_{1-x}\text{F}_4$ has also been much questioned over the years.^{43,44,45,49,50}

Notwithstanding that recent experimental work reports a SG transition in $\text{LiHo}_x\text{Y}_{1-x}\text{F}_4$ ($x=0.045$),⁴⁵ it is interesting to ask if difficulties in establishing the existence of a dipolar SG in strongly diluted $\text{Eu}_x\text{Sr}_{1-x}\text{S}$ ^{57,58} and in $\text{LiHo}_x\text{Y}_{1-x}\text{F}_4$, i.e. the suggested anti-glass phase at $x=0.045$ ^{43,47,48} or absence of signatures of SG transition both at $x=0.045$ and $x=0.165$,^{49,50} are related. A clearer picture of the formation of relatively large spin blocks below the percolation threshold that collectively form a cluster SG phase was obtained from experiments on $\text{Eu}_x\text{Ca}_{1-x}\text{B}_6$.⁵⁹ Clusters with magnetic moments $\mu \simeq 260\mu_B$ were observed and the transition temperature separating the cluster glass and paramagnetic phases, for Eu concentrations between around $x=0.1$ and $x=0.3$, was measured to be of order of 2 K.⁵⁹

Promising candidates for diluted dipolar Heisenberg SGs can be found among gadolinium compounds. Gd^{3+} ion has a half-filled $4f$ -shell. The ground state manifold is $^8S_{7/2}$ and with little orbital momentum contribution. Gd^{3+} is therefore a good approximation of a classical Heisenberg spin. Good example of materials that can be considered as candidates for diluted dipolar Heisenberg SGs are $(\text{Gd}_x\text{Y}_{1-x})_2\text{Ti}_2\text{O}_7$ and $(\text{Gd}_x\text{Y}_{1-x})_2\text{Sn}_2\text{O}_7$. $\text{Gd}_2\text{Ti}_2\text{O}_7$ and $\text{Gd}_2\text{Sn}_2\text{O}_7$ are strongly frustrated Heisenberg pyrochlore antiferromagnets.^{60,61,62} While the Curie-Weiss temperature is about $\theta_{\text{CW}} \sim -10$ K, due to frustration, both compounds remain disordered down to $T = 1$ K.^{60,63} Theoretically, the extensive ground-state degeneracy in the pyrochlore nearest-neighbor Heisenberg antiferromagnet prevents ordering down to zero temperature,^{64,65} and the low temperature order in the aforementioned materials is induced by other, weaker interactions that are specific to each of these compounds. One of the interaction at play below 1 K is the dipolar interaction. Indeed, in the case of $\text{Gd}_2\text{Sn}_2\text{O}_7$, the spin configuration in the ordered state was found⁶⁶ to be the ground state of the pyrochlore antiferromagnet with dipolar interactions.⁶⁷ In the case of $\text{Gd}_2\text{Ti}_2\text{O}_7$, other interactions, like further nearest-neighbor exchange, are likely at play. Indeed, below the first phase transition at 1 K, there is another one at 0.7 K,⁶³ with both phases ordered with propagation vector $k = [\frac{1}{2} \frac{1}{2} \frac{1}{2}]$.^{68,69}

Another candidate material, also well studied in the context of geometrical frustration, is the $\text{Gd}_3\text{Ga}_5\text{O}_{12}$ garnet (GGG). The cubic lattice structure of this frustrated Heisenberg antiferromagnet consist of two interpenetrating sublattices of corner-sharing triangles. While the Curie-Weiss temperature is $\theta_{\text{CW}} \sim -2$ K, the frustration postpones ordering down to 0.18 K.⁷⁰ The rich low temperature physics of GGG is still not fully understood, but some insight has been recently gained from dynamic magnetization studies, revealing that in the low temperature phase there is long-range order coexisting with both spin liquid^{71,72} and spin glass⁷³ behavior. In the framework of Gaussian mean-field theory, it was shown that the dipolar interaction plays an important role in the ordering in GGG,^{74,75} and that the neutron scattering data⁷⁰ can be reproduced with a proper

treatment of the dipolar interactions.^{74,75} Analogously to $(\text{Gd}_x\text{Y}_{1-x})_2\text{Ti}_2\text{O}_7$ and $(\text{Gd}_x\text{Y}_{1-x})_2\text{Sn}_2\text{O}_7$, at sufficient dilution, $(\text{Gd}_x\text{Y}_{1-x})_3\text{Ga}_5\text{O}_{12}$ may be expected to exhibit, at low temperature, a dipolar SG phase.

In the studies motivated by experiments indicating a SG freezing in frozen ferrofluids,⁴⁰ some evidence for a SG freezing in a system of dense amorphous Heisenberg and XY spins coupled by long-range dipolar interactions was obtained from molecular dynamics simulations.^{38,39} But no systematic investigation of the thermodynamic nature of the freezing was at that time really possible.

In the present work, in anticipation of eventual experimental studies of dipolar SG, e.g. diluted Gd compounds, or further work on $\text{Eu}_x\text{Sr}_{1-x}\text{S}$ or $\text{Eu}_x\text{Ca}_{1-x}\text{B}_6$, we perform numerical studies of the SG transition in a diluted dipolar Heisenberg model. At high dilution, the lattice structure should be irrelevant and data obtained for different systems should be comparable.⁷⁶ Here we consider the simplest possible geometry where we study dipoles randomly placed at the sites of SC cubic lattice. We provide Monte Carlo data that supports the scenario that, at low dipole concentration, the diluted dipolar Heisenberg model displays an equilibrium phase transition to a SG phase. We calculate the critical exponents ν and η for the SG transition in the model studied. The derived exponents do not match experimental or Monte Carlo exponents, neither for Heisenberg nor Ising SG. This may be because of important scaling corrections and severe restriction of the system sizes that we were able to study due to the computationally expensive summation of long-range dipole-dipole interaction and very slow equilibration.

The rest of the paper is organized as follows. In Section II, we define the model and MC method employed. In Section III, we introduce the observables calculated in the simulation. In Section IV, we present and discuss our results. Our conclusions are in Section V. Some technical details are discussed in Appendices. In Appendix A, we examine the temperature and system size dependence of the magnetization and staggered magnetization of the model studied. In Appendix B, we discuss the issue of the self-interaction term that must be taken into account when periodic boundary conditions are imposed. In Appendix C, we discuss the Ewald summation technique. In Appendices D and E, we discuss the overrelaxation and heatbath algorithms, respectively.

II. MODEL AND METHOD

A. Model

We consider a system that consists of classical three-component ($n=3$, Heisenberg) dipoles that are free to point in any direction. The dipoles are randomly distributed on the sites of a 3D simple cubic (SC) lattice.

The Hamiltonian is of the form

$$\mathcal{H} = \frac{1}{2}\epsilon_d \sum_{i \neq j} \sum_{\mu, \nu} \frac{\delta^{\mu\nu} r_{ij}^2 - 3r_{ij}^\mu r_{ij}^\nu}{r_{ij}^5} S^\mu(\mathbf{r}_i) S^\nu(\mathbf{r}_j), \quad (1)$$

where $S^\mu(\mathbf{r}_i)$ ($\mu = x, y, z$) denote Cartesian components of classical spin vectors, $\mathbf{S}(\mathbf{r}_i)$, which are of unit length, $|\mathbf{S}(\mathbf{r}_i)| = 1$. The energy scale of dipolar interactions is set by $\epsilon_d = \frac{\mu_0 \mu^2}{4\pi a^3}$, where μ is the magnetic moment of the spin $\mathbf{S}(\mathbf{r}_i)$, a is the lattice constant and μ_0 denotes vacuum permeability. Below, ϵ_d/k_B , where k_B is the Boltzmann constant, is conveniently used as a unit of temperature. The summation is carried over all occupied lattice sites and over the vector components of the spin, $\mu, \nu = x, y$ and z . The factor 1/2 is included to correct for double counting of dipole pairs. \mathbf{r}_i and \mathbf{r}_j are the positions of ions labeled i and j , respectively, and their distance, $|\mathbf{r}_{ij}| = |\mathbf{r}_j - \mathbf{r}_i|$, is measured in units of nearest-neighbor distance, a . We use periodic boundary conditions. In the case of long-range interactions, this means that to calculate a pairwise interaction, we must sum over an infinite array of dipole images replicated with a periodicity set by the dimensions of the simulation box. Therefore, it is convenient to consider the interaction constant for spins i and j as a 3 by 3 matrix, \hat{L}_{ij} . The matrix elements of \hat{L}_{ij} are denoted $L_{ij}^{\mu\nu}$, and for dipoles separated by a vector \mathbf{r}_{ij} , are given by the sum,

$$L_{ij}^{\mu\nu} = \sum_{\mathbf{n}} \frac{\delta^{\mu\nu} |\mathbf{r}_{ij} + \mathbf{n}|^2 - 3(\mathbf{r}_{ij} + \mathbf{n})^\mu (\mathbf{r}_{ij} + \mathbf{n})^\nu}{|\mathbf{r}_{ij} + \mathbf{n}|^5}. \quad (2)$$

Vectors \mathbf{n} are of the form $\mathbf{n} = L(k\hat{x} + l\hat{y} + m\hat{z})$, where k, l, m are integers and \hat{x}, \hat{y} and \hat{z} are the unit vectors pointing in the directions of primitive translation vectors of the SC lattice. L is an integer expressing the size of the simulation cell in units of the lattice constant, a . Note that, in a simulation, care must be taken to correctly include the so-called self-interaction term, \hat{L}_{ii} , (see Appendix B). The self-interaction term originates from interaction of spin with its periodic images replicated outside the simulation cell. The lattice summation (2) is performed using the Ewald technique;^{77,78,79,80} the details of which are given in Appendix C. The calculated Ewald sums correspond to a summation over a long cylinder, such that the demagnetization field is zero. Using interaction constants defined in Eq. (2), the Hamiltonian can then be written in the form

$$\mathcal{H} = \frac{1}{2}\epsilon_d \sum_{i,j} \mathbf{S}(\mathbf{r}_i) \hat{L}_{ij} \mathbf{S}(\mathbf{r}_j). \quad (3)$$

The summation in Hamiltonian (3) includes only the spins enclosed in the simulation cell, while the presence of spins outside the simulation box is approximated by periodic images of the spins within the simulation cell, and this effect is included in the interaction constants, given by the matrix \hat{L}_{ij} calculated via the Ewald method. Note that, unlike in Eq. (1), the self-interaction terms, $i = j$, are included in the summation (3).

B. Method

Our simulations employ the standard single spin-flip Metropolis Monte Carlo algorithm with parallel tempering (PT).^{81,82} PT was found to significantly speed up equilibration in slowly relaxing systems.^{81,82} In this technique, one simultaneously simulates a number, N_T , of thermal replicas - copies of the system with the same spatial disorder, but at different temperatures. In each thermal replica, the simulation begins from a different random initial spin configuration. At every 10 local update sweeps, each consisting of N single spin updates, where N is the number of spins in the system, a configuration swap among thermal replicas is attempted with the acceptance probability preserving the detailed balance condition. The frequency of tempering is chosen to balance the following two factors. As thermal tempering is computationally inexpensive, it is desirable to perform replica swap attempts often, to promote traveling of the replicas along the temperature axis. But, on the other hand, after a parallel tempering induced configuration exchange, a sufficient number of local update sweeps has to be performed to let the new configuration evolve at the given temperature. If a subsequent tempering is attempted too soon, the two configurations could be swapped back, and in that case no progress in the relaxation of a state trapped in a local energy minimum would have been made. The number of thermal replicas, N_T , and simulated temperatures, T_α , where $\alpha = 1, \dots, N_T$, are chosen to yield a sufficiently high and temperature independent PT configuration swap acceptance rate, i.e. not less than 50%. A uniform with respect to temperature, T_α , PT acceptance rate is achieved by choosing T_α to satisfy the formula²³

$$(T_\alpha - T_{\alpha-1})/T_\alpha = 1/\sqrt{C_V N}, \quad (4)$$

where N denotes the number of dipoles. The specific heat per spin, C_V , used in Eq. (4) was measured in preliminary simulations of the smallest system sizes, with uniformly distributed temperatures.

The Metropolis single-spin moves are attempted within a temperature-dependent solid angle, where the angle is self-consistently chosen such that the acceptance rate of MC single spin move is close to 50%. To carry out a spin move, we choose a coordinate system with the \hat{z} axis along the current spin direction, and randomly choose a polar angle, θ , and azimuthal angle, ϕ . In order to obtain a uniform distribution of random points on a unit sphere one needs to draw ϕ and $z = \cos(\theta)$ from a uniform probability distribution, such that $\phi \in (0, 2\pi)$ and $z \in (-1, 1)$. Here, to maintain the desired acceptance rate, the move is restricted to a limiting angle, θ_{\max} , relative to the initial spin direction; hence, the choice of z is restricted to $z \in (1 - z_{\max}, 1)$, where $z_{\max} = \cos(\theta_{\max})$. To obtain z_{\max} such that the acceptance rate, p_{acc} , is 50%, during each 100 MCS p_{acc} is measured, and afterwards z_{\max} is adjusted. If p_{acc} is lower than 0.5, z_{\max} should be decreased; in the opposite case, when $p_{\text{acc}} > 0.5$,

L	N_{dip}	N_{samp}	N_{eq}	N_{prod}	N_{T}	T_{min}	T_{max}
$x=0.0625$							
8	32	5000	$5 \cdot 10^5$	$5 \cdot 10^5$	16	0.05	0.1763
10	62,63	2000, 2000	$2 \cdot 10^6$	10^6	16	0.05	0.1763
12	108	1200	10^7	10^6	16	0.05	0.1763
14	172	1000	10^7	10^6	16	0.05	0.1763
$x=0.125$							
6	27	3000	$5 \cdot 10^5$	$5 \cdot 10^5$	16	0.0750	0.2869
8	64	2000	$2 \cdot 10^6$	10^6	16	0.0750	0.2869
10	125	1500	$2 \cdot 10^6$	10^6	16	0.0800	0.2811
12	216	1000(+200)	$5 \cdot 10^6(2 \cdot 10^7)$	10^6	16	0.0850	0.2787

Table I: Parameters of the Monte Carlo simulations for two dipole concentrations, x . L is the linear size of the simulation box; N_{dip} is the number of spins, and N_{samp} denotes number of disorder samples. N_{eq} and N_{prod} are the number of MCS in the equilibration and measurement phase of the simulation, respectively. N_{T} is the number of thermal replica and T_{min} , T_{max} are the lowest and highest temperatures in PT scheme. For $L=10$, $x=0.0625$, to obtain the desired x , two numbers of dipoles were simulated, and the disorder average was taken over the results for both $N_{\text{dip}} = 62$ and $N_{\text{dip}} = 63$. For $L=12$, $x=0.125$ the numbers given in round brackets pertain to a subset of disorder replicas simulated longer, to monitor equilibration; the long equilibration time results for these replicas were included in the disorder averaging.

z_{max} should be increased, while for $p_{\text{acc}} = 0.5$, z_{max} does not change. Such update of z_{max} can be obtained when multiplying the current value of z_{max} , $z_{\text{max}}^{(\text{old})}$, by $2p_{\text{acc}}$; hence, a new value of z_{max} is calculated according to the formula $z_{\text{max}}^{(\text{new})} = 2p_{\text{acc}}z_{\text{max}}^{(\text{old})}$, with the restriction $z_{\text{max}}^{(\text{new})} \in (0.001, 2)$. After choosing ϕ and θ , that is a new spin direction in the coordinates relative to the initial spin direction, a transformation to the global coordinate system is performed.

We simulated two dipole concentrations, $x = 1/16 = 0.0625$ and $x = 1/8 = 0.125$, and for each concentration we considered 4 system sizes varying between around 30 and 200 dipoles, which is the largest size that we were able to equilibrate. To perform the necessary disorder average (see Section III), we considered at least 1000 disorder samples. The parameters of the simulations are collected in Table I. To generate results reported here, we used in total around $3 \cdot 10^5$ hours (~ 35 years) of CPU time on AMD Opteron, 2.6 GHz. The statistical error is based on disorder sampling fluctuation and is calculated using the standard jackknife method.^{83,84,85}

To reduce the number of performed lattice sums, for each lattice site k we calculate the local interaction field,

$$\mathbf{H}_k = \sum_{j \neq k} \hat{L}_{kj} \mathbf{S}_j, \quad (5)$$

and update it only when the spin change is accepted. Having \mathbf{H}_k available, the computational complexity of calculating the energy change when a single spin is

moved, which is needed to test if the spin move is accepted, is of order of a small constant number of arithmetic operations, $\mathcal{O}(1)$. As the field, \mathbf{H}_k , is updated only if the spin move is accepted, the computational cost of updating the local field, \mathbf{H}_k , which is $\mathcal{O}(N)$, is avoided if the spin move is rejected. In consequence the computational cost of rejected Metropolis spin updates is negligible.

It was reported that the autocorrelation time can be substantially decreased in simulations of Heisenberg SG by performing computationally inexpensive overrelaxation (microcanonical) spin updates.^{86,87} Overrelaxation updates are zero-energy spin moves that consist of 180 degrees rotation of the spin around the local molecular field. Including overrelaxation moves in simulations of short-range Heisenberg spin systems is beneficial because overrelaxation moves are faster than Metropolis updates. Here, in the case of long-range interaction, the computational cost of overrelaxation moves would not be less than the cost of Metropolis spin flips, as most of the time is spent on updating the local interaction field (5), and the local interaction field has to be updated both after an accepted Metropolis spin flip and after an overrelaxation move. Furthermore, it is worth to note that in the general case of non-cubic geometry with periodic boundary conditions, where the self-interaction term is present (see Appendix B), an overrelaxation move does not preserve the energy (see Appendix D).

In the case of the nearest-neighbor Heisenberg SG model, it is more efficient to use the heatbath algorithm^{88,89,90} for local spin updates. In the heatbath algorithm spins are individually connected to a heatbath, i.e. a new spin direction, which is independent from the previous direction, is drawn from the Boltzmann probability distribution for a spin in the local molecular field, \mathbf{H}_k . Hence, in contrast to the conventional Metropolis method, in the heatbath algorithm, the computational cost of rejected spin moves is avoided. For the current problem, the benefit of using the heatbath algorithm would not be high because the computational cost of rejected spin update attempts is negligible in comparison with the computational cost of accepted updates which require recalculating the lattice sums in Eq. (5). Also, similarly to the case of overrelaxation moves, if the geometry of the simulation cell is not cubic, the self-interaction term in the Hamiltonian introduced by the periodic boundary conditions makes the heatbath algorithm impractical (see Appendices B and E). So, while we are considering here a cubic system, in order to keep our method general and to obtain results that are the easiest to compare with possible future simulations with different lattice geometries, we decided to not use the heatbath algorithm nor overrelaxation moves in this work.

III. PHYSICAL QUANTITIES

In spin-glass systems, the order parameter can be defined as an overlap between two independent, identical copies of the system. In the case of 3D Heisenberg spins, the overlap can be calculated for 9 combinations of the vector components. We write

$$q^{\mu\nu}(\mathbf{k}) = \frac{1}{N} \sum_{\mathbf{r}} S_{\mu}^{(\alpha)}(\mathbf{r}) S_{\nu}^{(\beta)}(\mathbf{r}) \exp(i\mathbf{k} \cdot \mathbf{r}), \quad (6)$$

where $\mu, \nu = x, y, z$ and where α and β denote different copies of the system with the same random disorder and that are simulated simultaneously, but independently. The wave-vector-dependent SG order parameter is

$$q(\mathbf{k}) = \sqrt{\sum_{\mu, \nu} |q^{\mu\nu}(\mathbf{k})|^2}. \quad (7)$$

In the case of EA Heisenberg SG, in addition to spin, a chirality variable^{18,19} is also considered,^{19,20,21,22,23,24,25,26} and the chirality overlap order parameter and further quantities defined using this order parameter are calculated. Here, for a diluted dipolar Heisenberg SG, we do not consider chirality. The chirality cannot be easily defined in a diluted system. Moreover, note that, as discussed in the Introduction, the anisotropy of the dipolar interaction, in the presence of spatial disorder, brakes the rotational symmetry. Because of that, the chirality, if it was defined, cannot be decoupled from the spin.

Traditionally, the finite-size scaling (FSS) analysis of SG simulation data has been based on the calculation of Binder ratios,^{91,92,93} which, for an $n=3$ Heisenberg SG, is defined as:^{24,26}

$$U_L = \frac{1}{2} \left(11 - 9 \frac{[\langle q(0)^4 \rangle]}{[\langle q(0)^2 \rangle]^2} \right), \quad (8)$$

where $\langle \dots \rangle$ denotes thermal averaging and $[\dots]$ is a disorder average. The numerical factors in Eq. (8) are chosen such that at $T = \infty$, assuming Gaussian distribution of $q(0)$, $U_L = 0$, and at $T = 0$, where $q(0)$ is not fluctuating, U_L is 1. Being a dimensionless quantity, U_L is expected to display FSS properties described by¹²

$$U_L = \tilde{X}(L^{1/\nu}(T - T_g)), \quad (9)$$

where the scaling function⁹⁴ \tilde{X} is an analytic function of its argument, and ν is the universal correlation length exponent, such that there is no system size dependence outside the argument of the scaling function. Many recent works report that in the case of disordered spin glass systems, a better FSS analysis can be achieved when considering the finite-size SG correlation length, ξ_L .^{11,23,46,96} In the context of Ising SGs, it was suggested that U_L may not cross due to a lack of unique ground state⁹⁶ or because it is too noisy (see footnote Ref. [97]),¹¹ being a

quantity that requires evaluation of a four-point correlation function, as opposite to ξ_L , that is defined using a two-point correlation function. It was also observed that scaling corrections are larger for U_L than for ξ_L .¹¹ It is likely that in the case of Heisenberg SG large scaling corrections are the leading factor behind the lack of crossing of the Binder ratios. To proceed, we define the SG susceptibility^{8,11,23} as

$$\chi_{\text{SG}}(\mathbf{k}) = N [\langle q(\mathbf{k})^2 \rangle]. \quad (10)$$

Assuming an Ornstein-Zernike form for the SG susceptibility,⁹⁸

$$\chi_{\text{SG}}(\mathbf{k}) \propto 1/(|\mathbf{k}|^2 + \xi^{-2}), \quad (11)$$

where $|\mathbf{k}| \ll 1/\xi$. We define a finite-size SG correlation length,^{11,99} ξ_L , via

$$\xi_L = \frac{1}{2 \sin(k_{\min}/2)} \left(\frac{\chi_{\text{SG}}(0)}{\chi_{\text{SG}}(\mathbf{k}_{\min})} - 1 \right)^{1/2}. \quad (12)$$

The correlation length divided by the system dimension, ξ_L/L , similarly to the Binder ratio, is a dimensionless quantity that is expected to scale according to the relation^{11,12,23,26}

$$\xi_L/L = \tilde{Y}(L^{1/\nu}(T - T_g)), \quad (13)$$

where \tilde{Y} is once again a scaling function. Hence, at a putative SG transition temperature, T_g , ξ_L/L is expected to be size independent.

IV. MONTE CARLO RESULTS

A system of Heisenberg dipoles on a fully occupied SC lattice orders antiferromagnetically.^{100,101} To rule out a long-range order in the simulated diluted systems, we calculated the magnetization, M , and the staggered magnetization, M_{stag} . Both M and M_{stag} are small and decrease with increasing system size. This indicates that their nonzero value is a finite-size effect and not a result of long-range ordering. More detailed discussion of M and M_{stag} is given in Appendix A.

We plot in Fig. 1 the temperature dependence of the Binder ratio, U_L , for $x=0.125$ and $x=0.0625$, for different system sizes. The Binder ratio curves do not cross; hence, they do not provide indication of a phase transition. Also, in some studies of other models, a crossing of the Binder ratios was not found, while the scaling invariance of the finite-size correlation length was established, indicating a transition to a SG phase. The magnitude of scaling corrections is different for different observables and they are likely to be larger for Binder ratio than for correlation length. In the simulation of the Ising EA SG^{11,12} U_L does cross, but the scaling corrections are found to be larger for U_L than for ξ_L/L .¹¹ In the case of the site diluted EA Ising SG,¹⁰² where scaling corrections are large in comparison with other Ising SG models,

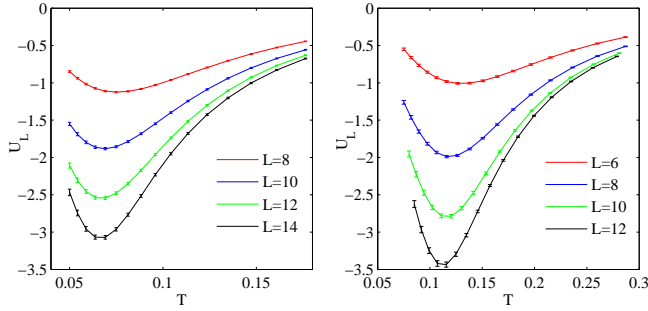


Figure 1: (color online). Binder ratios for $x=0.0625$ (left) and $x=0.125$ (right) as a function of temperature.

ξ_L/L plots are crossing with large shifts between system sizes, while the U_L curves do not cross, but merge at low temperature. A similar effect has been seen in the studies of diluted dipolar Ising SG^{46,52} - U_L plots do not cross, but they have a tendency to merge at low T , while ξ_L/L plots intersect.⁴⁶ In the case of isotropic Heisenberg EA SG,^{24,25,26} the behavior of spin and chirality Binder ratios differs, but neither show a crossing, while the correlation length shifts between system sizes shows that scaling corrections are large. It is worthwhile to note that the form of Binder ratio plots, characterized by a dip to a negative value in the proximity of T_g , resembles the Binder ratio plots for chirality (and not spin) in the Heisenberg EA model,^{24,26} or the Binder ratio plots for spin in Heisenberg SG models in the presence of random anisotropy in three¹⁰³ and four¹⁰⁴ dimensions.

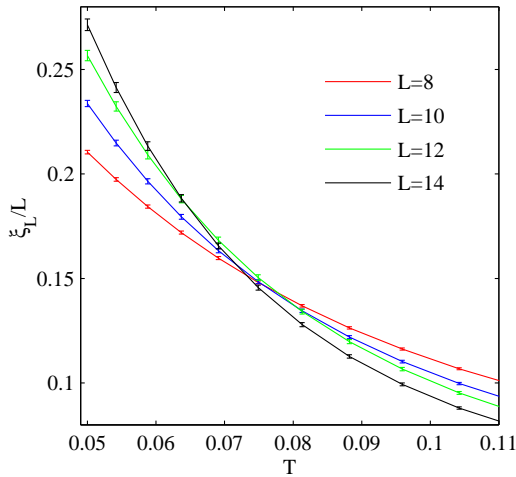


Figure 2: (color online). SG correlation length as a function of temperature, $x=0.0625$.

Having discussed the temperature dependence of the Binder ratios, we now turn to the behavior of the SG correlation length, $\xi_L(T)$. We show the plots of ξ_L/L vs T for various system sizes in Figs. 2 and 3. The curves do cross; but, for both concentrations, there are large shifts

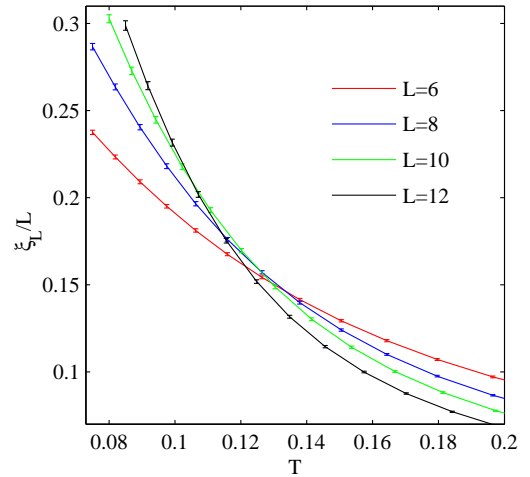


Figure 3: (color online). SG correlation length as a function of temperature, $x=0.125$.

between the intersection points for different system sizes. The large shifts between the intersection points were also found in the studies of the EA Heisenberg SG.^{24,25,26} In the case of EA Heisenberg SG, a broad range of system sizes were studied and the shifts between the intersection points were systematically analyzed.^{24,25,26} The limitation with our data, which are due to time consuming summation of long range interactions, prevent us from investigating large system sizes and, therefore, to perform such an analysis. Because of a narrow range of available system sizes, the separation between the curves in the crossing region is small in comparison with the errorbars. Hence, the statistical uncertainty of locating the crossing points would be large. Indeed, looking at Figs. 2 and 3 one realizes that by moving the curves within the error bars, the position of the crossing can be changed substantially. Also, the number of system sizes and, consequently, the number of intersection points is small. In our ξ_L/L vs T data, the shifts between the intersection points for the smallest system sizes, consistently for both concentrations, are much smaller than the shift of the intersection point of the two largest system sizes studied. Such feature have not been found in simulations of EA Heisenberg SG.^{24,25,26} A possible explanation for such behavior may be existence of short-range ferromagnetic correlations. Such a ferromagnetic spin blocking would especially strongly affect the data for the smallest system sizes, which possibly have the linear dimensions comparable with the length scale of the short-range ferromagnetic correlations. Spin blocking has been observed experimentally in studies of diluted dipolar Heisenberg systems $\text{Eu}_x\text{Sr}_{1-x}\text{S}$ ^{57,58} and $\text{Eu}_x\text{Ca}_{1-x}\text{B}_6$.⁵⁹ Another argument supporting short range ferromagnetic correlations scenario in the model studied herein is the finite-size magnetization found for small system sizes (see Appendix A).

The scaling equation (13) is expected to be satisfied

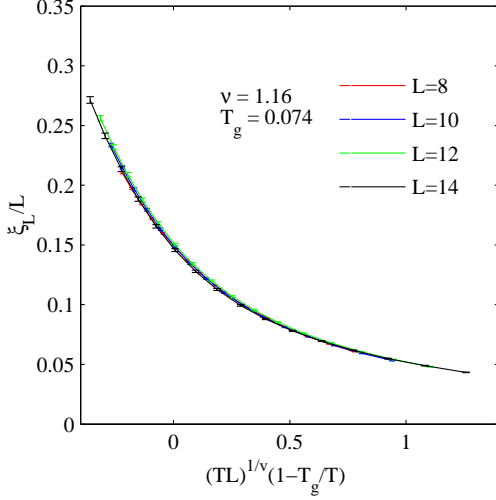


Figure 4: (color online). Extended scaling of ξ_L/L at $x=0.0625$

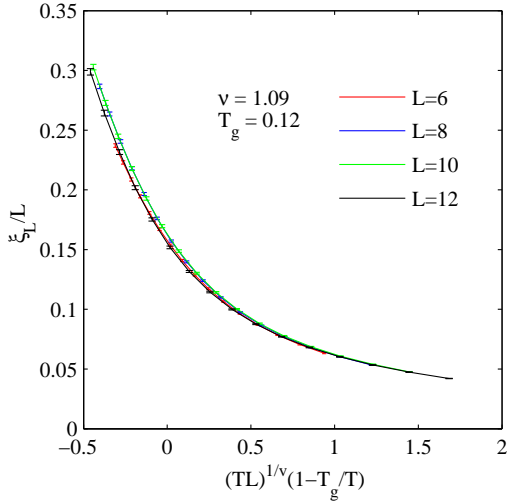


Figure 5: (color online). Extended scaling of ξ_L/L at $x=0.125$

only in close proximity of T_g . To better describe the data at a larger distance from the critical point, Campbell *et al.* proposed a heuristic extended scaling scheme (ESS)¹⁰⁵ for ξ_L/L of the form:

$$\xi_L/L = \tilde{Y} \left((TL)^{1/\nu} \left(1 - \frac{T_g}{T} \right) \right), \quad (14)$$

and showed the improvement of the accuracy it provides in the case of a 2D Ising ferromagnet. Based on the assumption of a symmetric interaction distribution, $P(J_{ij})$, they proposed, and tested numerically, an alternative scaling formula for the Ising EA spin glass, where T_g/T in Eq. (14) is replaced with $(T_g/T)^2$. Here we use the scaling formula of Eq. (14) because the bond distribution in the case of diluted dipoles is not symmetric. In a recent MC simulation of a diluted dipolar Ising SG, an ESS as given

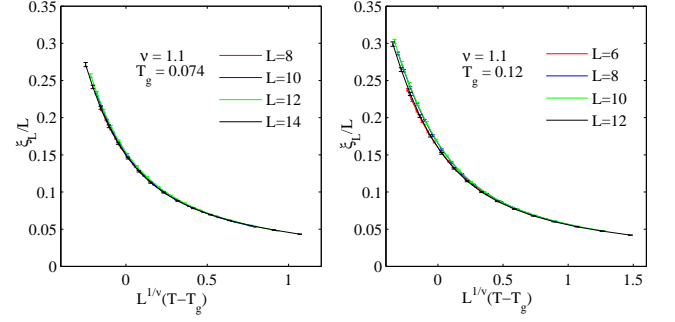


Figure 6: (color online). Conventional scaling of ξ_L/L with $L^{1/\nu}(T - T_g)$; $x=0.0625$ (left) and $x=0.125$ (right).

by (14) was also found to describe the scaling of ξ_L/L better than if $(T_g/T)^2$ was used.⁴⁶

We fit our data for ξ_L/L to the scaling function (14) over the whole simulated temperature range, shown in Table I. The scaling function, \tilde{Y} , is approximated with a 6th order polynomial,

$$F(z) = \sum_{m=0}^6 a_m z^m, \quad (15)$$

where $z = (TL)^{1/\nu}(1 - T_g/T)$. We define the penalty function,

$$D = \sum_{\text{MC data}} (F(z)L/\xi_L - 1)^2, \quad (16)$$

that is minimized with respect to the parameters $\{a_m\}$, T_c and ν . We obtain the values of the critical exponent $\nu=1.16$, $\nu=1.09$, and transition temperatures $T_g=0.074$, $T_g=0.12$ for $x=0.0625$ and $x=0.125$, respectively. The scaling collapse of the simulation data is shown in Fig. 4 and Fig. 5.

In Figs. 6 and 7, just for comparison, we present the results of the fitting to the conventional formula (13) and ESS with $(T_g/T)^2$. The fitting to the conventional formula (13), shown in Fig. 6, gives quite similar results to the ESS of Eq. (14). Apparently, the inaccuracy due to the small system sizes studied is larger here than the correction made by replacing Eq. (13) with Eq. (14).

In the case of fitting to Eq. (14) with $(T_g/T)^2$, we obtain a visibly worse data collapse than when T_g/T is used; the result of such a fit is shown in Fig. 7.

We plot in Figs. 8 and 9 the SG susceptibility for $\mathbf{k} = 0$, $\chi_{\text{SG}}(0)$, of Eq. (10) for $x=0.0625$ and $x=0.125$, respectively.

The SG susceptibility is expected to scale according to the ESS formula¹⁰⁵

$$\chi_{\text{SG}} = (TL)^{2-\eta} \tilde{Z} \left((TL)^{1/\nu} \left(1 - \frac{T_g}{T} \right) \right), \quad (17)$$

We performed a fit following a procedure similar to the method used for the scaling fit of ξ_L/L described in

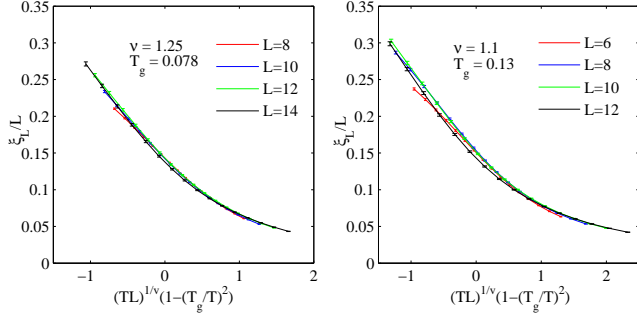


Figure 7: (color online). Extended scaling of ξ_L/L with $(TL)^{1/\nu}(1-(T_g/T)^2)$; $x=0.0625$ (left) and $x=0.125$ (right).

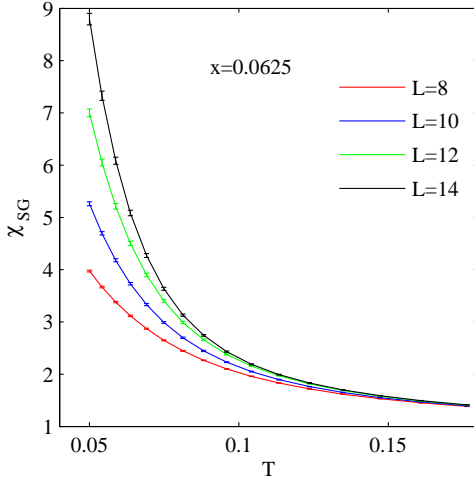


Figure 8: (color online). SG susceptibility, $x=0.0625$

Eqs. (15) and (16). For $x=0.0625$ we obtain $T_g = 0.078$, $\nu=1.25$ and $\eta=1.45$. For $x=0.125$ we get $T_g = 0.12$, $\nu=1.18$ and $\eta=1.35$. The critical temperatures are consistent with those obtained from FSS of ξ_L/L . The values of the critical exponent ν obtained here are slightly larger than ν obtained from the scaling of ξ_L/L . The scaling collapse of χ_{SG} is plotted in Fig. 10 and 11 for $x=0.0625$ and $x=0.125$, respectively.

In the dipolar Hamiltonian (1) off-diagonal terms, that couple different vector components of the dipolar moment, are present. The off-diagonal terms destroy the rotational ($O(3)$) symmetry in an otherwise isotropic vector spin system, and only a Z_2 symmetry remains. It was suggested that such spatially disordered dipolar systems belong to the Ising universality class.^{17,54} Due to spatial disorder, the couplings, including the off-diagonal terms, are random, and the distribution of local freezing direction in the SG phase remains uniform, unlike in a system with a global single-ion anisotropy (e. g. $-DS_z^2$ term in the Hamiltonian). With the uniform distribution of local freezing directions, a system is said to have a statistical

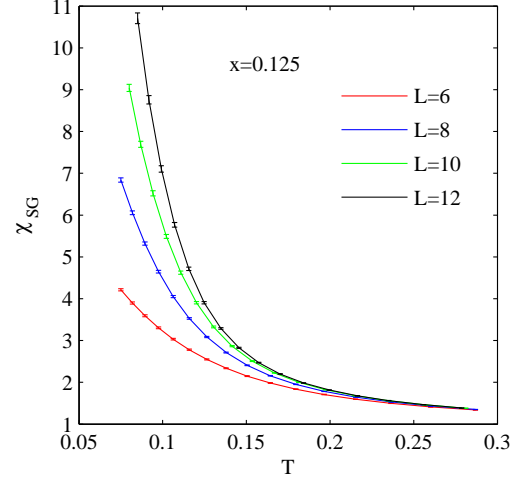


Figure 9: (color online). SG susceptibility, $x=0.125$

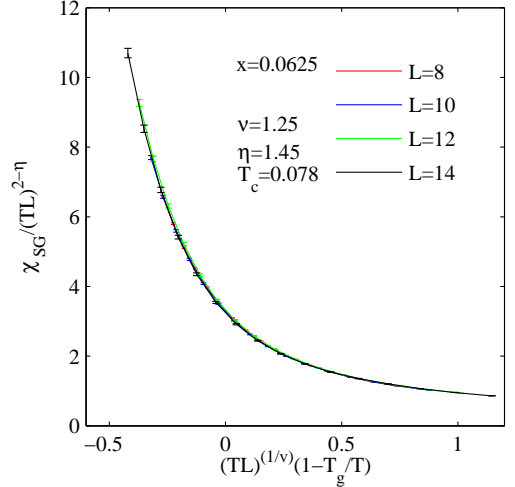


Figure 10: (color online). SG susceptibility scaling, $x=0.0625$

rotational symmetry.¹⁷

The values of the critical exponents found in this work do not agree with either those from simulations of short-range Ising SG, $\nu = 2.45$, $\eta = -0.375$,¹³ nor Heisenberg SG, $\nu = 1.49$, $\eta = -0.19$.²⁶ It is possible that our exponent ν is consistent with $\nu = 1.3$ and $\nu = 0.95$ obtained for Ising diluted dipolar SG in Ref. [46] and Ref. [53], respectively. Extracting SG critical exponents from simulations is difficult. Critical exponents for the Ising SG have been discussed for a long time^{9,10,11,12,13,14}, and proposed values were changing much with progress in development of simulation algorithms and computer hardware. Similarly to the early simulations of the Ising SG,^{9,10} our data very likely suffer from large scaling corrections. As our system sizes are small, one may want to compare our exponent ν with the results of simulations of the Ising SG performed for small system sizes, e.g. these in Ref. [9]

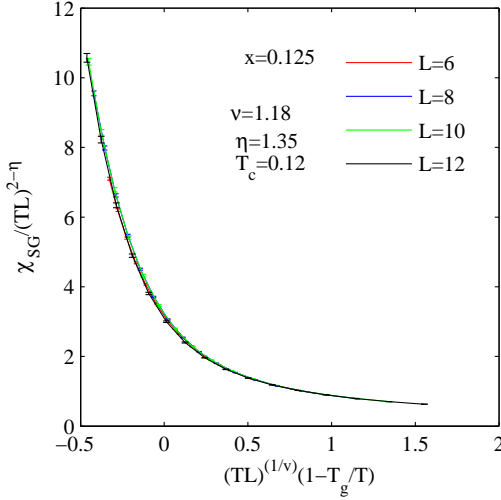


Figure 11: (color online). SG susceptibility scaling, $x=0.125$

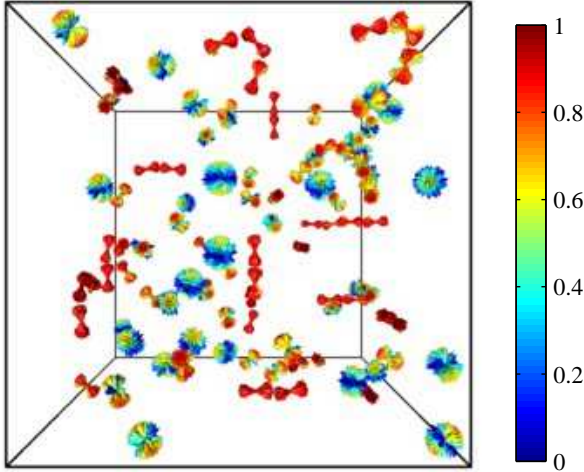


Figure 12: (color online). Snapshot of 200 equilibrated independently spin configurations for $L=12$, at $T=0.05$ and $x=0.0625$. The alignment, i.e the scalar product, of the spins with the local freezing axes is indicated by the colors of arrows.

($\nu = 1.2$) or Ref. [10] ($\nu = 1.3$). There is a fair agreement in ν but not in η . The value of the exponent η , from simulation^{11,12,13,26} and experiments^{4,31,32} on many different materials, for both Ising and Heisenberg SG is a small number, either positive or negative but not exceeding 0.5 in absolute value. Surprisingly, the value of η we obtain for the diluted dipolar Heisenberg SG, $\eta = 1.4$, is much larger.

Having discussed the question of universality class and commented on the expectation that, for diluted $n=3$ component dipoles, it should be Ising, it is interesting to ask whether such Ising structure is explicitly physically manifest in the low temperature regime of the sys-

tems studied above. We show in Fig. 12 a number of super imposed snapshots of the spin configurations for one disorder realization, in the low temperature phase, at $T=0.05$, and dipole concentration $x=0.0625$. The image contains the spin configurations of 200 replicas of the same disorder, each equilibrated independently, starting from different random initial configuration. The system size is $L=12$, which, at the concentration $x=0.0625$, gives $N=108$ ions. The parameters of the simulations, i.e. temperatures and number of equilibration sweeps, are given in Table I. In the case of isotropic Heisenberg models, a low temperature phase has $O(3)$ rotational symmetry, and one expects the spin directions in replicas of the same disorder as explained above to be uniformly distributed. Here, due to the anisotropic character of the dipolar interactions, a subset of the dipoles is characterized by a unique Ising local freezing direction. It is indicated by the fact that in the snapshots some dipoles have a strong tendency to point along a particular local *random* direction, i.e the arrows can be enclosed by a circular conical surface with a small opening angle. Such inhomogeneous “random Ising structures” have also been observed in a model of diluted two-component 2D quadrupoles. For clarity, the alignment of spins with the local freezing directions, which is measured as an absolute value of the scalar product of a spin and the local freezing direction, is indicated by the color of the arrows. The local freezing direction vector is computed by summing all the spin vectors at a given site for the 200 disorder realizations in the following way. Starting from the second element in the sum, it is checked if adding another vector to the existing sum will increase or decrease the magnitude of the new sum. If adding the new element is to decrease the magnitude of the sum, the spin vector is added with a minus sign, such that the magnitude of the sum always increases. In this way we obtain a vector that is pointing along the local freezing axis. Not all the sites are characterised by a local freezing direction. The arrows on the sites that do not have a local freezing direction create spherical structures. These dipoles have freedom to point in any direction in the low temperature phase. That means that these dipoles are strongly frustrated and decoupled from the other dipoles. It is interesting to note that this behavior resembles the presence of “protected degrees of freedom” observed in gadolinium gallium garnet (GGG).⁷² The sites with a local freezing direction, in Fig. 12, seem to form small clusters. Possibility of ferromagnetic spin blocking was mentioned earlier as a potential explanation of a large shift of the correlation length crossing points for the largest system sizes relative to the crossing points for the smaller sizes. Formation of ferromagnetic spin blocks is also suggested by nonzero, but decreasing with system size, finite-size magnetization (see Appendix A).

In the simulations of a SG system, it is of paramount importance to ensure equilibration of the system before the statistics for the measured observables is collected. As the quantity of foremost interest here is the correla-

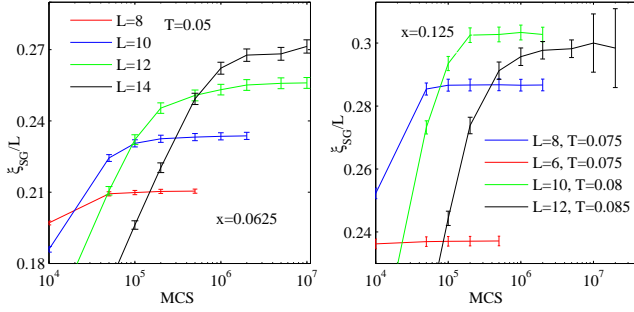


Figure 13: (color online). Equilibration $x=0.0625$ (left) and $x=0.125$ (right).

tion length, we assume that the system is equilibrated when the correlation length reaches a stationary state. We plot in Fig. 13 ξ_L/L vs the number of the equilibration steps performed before the measurement was taken. The number of necessary equilibration steps increases very rapidly with the system size and, because of this, we were only able to equilibrate system sizes up to about 200 dipoles. We observe that the long-range dipolar Heisenberg SG takes longer time to equilibrate than the short-range 3D EA Heisenberg SG model.^{24,26} A similar fact has been observed in the case of dipolar Ising SG.⁴⁶

V. SUMMARY

In conclusion, we have studied the spin-glass (SG) transition in a diluted dipolar Heisenberg model. From an analysis of the finite-size scaling of the SG correlation length, ξ_L , we found an indication of a SG transition at a temperature $T_g=0.074$, $T_g=0.12$, and critical exponent $\nu=1.16$, $\nu=1.09$ for dipole concentrations $x=0.0625$ and $x=0.125$, respectively. From finite-size scaling of the SG susceptibility, χ_{SG} , we obtained $T_g=0.078$, $\nu=1.25$, $\eta=1.45$, and $T_g=0.12$, $\nu=1.18$, $\eta=1.35$ for $x=0.0625$ and $x=0.125$, respectively. As in the isotropic Heisenberg SG, the Binder ratios, U_L , do not exhibit a crossing for different system sizes.

Our data support the scenario of ferromagnetic spin blocking. Short-range ferromagnetic correlations are indicated by a relatively large finite-size magnetization. Such short-range correlations would also explain unusual behavior of the SG correlation length ξ_L . The crossing points of the ξ_L/L vs T plots for the largest system sizes is shifted to much lower temperatures from the crossing points for the smaller system sizes. It may be caused by reaching a system size that is larger than the length scale of ferromagnetic clustering. Some indication of formation of frozen spin clusters can be also found from inspection of spin configuration snapshots.

The long-range interactions, and hence the large number of interacting spin pairs, give rise to a larger level of random frustration than in short-range (nearest neighbor)

bor) SG. Diluted dipolar SG seems to be more difficult to equilibrate than nearest-neighbor models. For example, we performed 10^7 Monte Carlo sweeps to equilibrate a system of around 200 dipoles. To compare, with the case of the Heisenberg Edwards-Anderson spin glass, around 10^7 Monte Carlo sweeps, with both overrelaxation and heatbath sweeps counted as a Monte Carlo sweep, were used to equilibrate a system of 32,768 spins.²⁵ In simulations of the Ising Edwards-Anderson spin glass around $6.5 \cdot 10^6$ Monte Carlo sweeps were used to equilibrate a system of 8000 spins.¹¹ Further progress in exploring the freezing in Ising^{46,53} and Heisenberg (this work) dipolar spin glasses will necessitate more sophisticated methods. We hope that our present work motivate such developments.

Acknowledgments

We thank Ka-Ming Tam and Paul McClarty for useful discussions. This work was funded by NSERC, the CRC Program (M. G., Tier 1). The calculations were made possible by dedicated resource allocation and the facilities of the Shared Hierarchical Academic Research Computing Network (SHARCNET:www.sharcnet.ca).

Appendix A: MAGNETIZATION AND STAGGERED MAGNETIZATION

As system of dipoles placed on the fully occupied SC lattice, or when the fraction of vacant sites is sufficiently low, orders antiferromagnetically.^{100,101} To rule out the presence of a long-range order we calculate the magnetization and staggered magnetization. The thermal and disorder averaged magnitude of magnetization is defined as

$$M = \left[\left\langle \left| \frac{1}{N} \sum_{i=1}^N \mathbf{S}_i \right| \right\rangle \right], \quad (\text{A1})$$

where $\langle \dots \rangle$ denotes thermal averaging and $[\dots]$ is a disorder average.

The antiferromagnetic ground state (GS) of a system of dipoles on fully occupied SC lattice is described by a spin vector with the following components:^{100,106}

$$\begin{aligned} S_i^x &= \tau_i^x \sin \theta \cos \phi, \\ S_i^y &= \tau_i^y \sin \theta \sin \phi, \\ S_i^z &= \tau_i^z \cos \theta, \end{aligned} \quad (\text{A2})$$

Such GS has two global rotational degrees of freedom: polar angle, θ , and azimuthal angle, ϕ . The sublattice and direction indexing vector, $\boldsymbol{\tau}_i \equiv [\tau_i^x, \tau_i^y, \tau_i^z]$, is given by

$$\boldsymbol{\tau}_i = [(-1)^{r_i^y + r_i^z}, (-1)^{r_i^x + r_i^z}, (-1)^{r_i^x + r_i^y}], \quad (\text{A3})$$

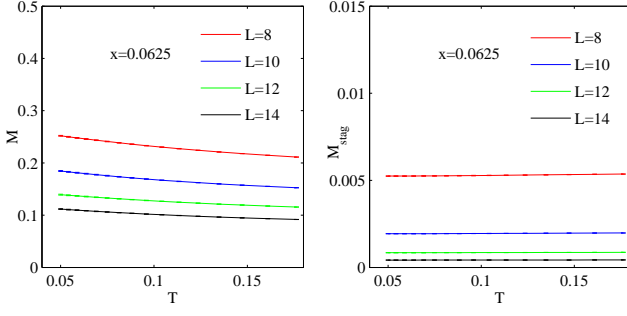


Figure 14: (color online). Magnetization, M , and staggered magnetization, M_{stag} , $x=0.0625$.

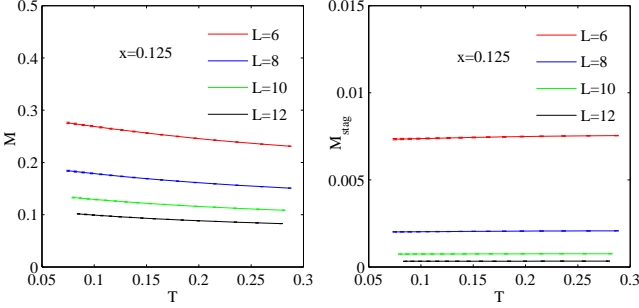


Figure 15: (color online). Magnetization, M , and staggered magnetization, M_{stag} , $x=0.125$.

where \mathbf{r}_i is the position of site i , measured in units of lattice constant, and its vector components, r_i^x , r_i^y and r_i^z , on SC lattice, are all integers. The staggered magnetization, which is indicating ordering described by Eqs. (A2), using sublattice and direction indexing vector $\boldsymbol{\tau}_i$ of Eq. (A3), is given by

$$M_{\text{stag}} = \left[\left\langle \left| \frac{1}{N} \sum_{i=1}^N \mathbf{S}_i \cdot \boldsymbol{\tau}_i \right| \right\rangle \right]. \quad (\text{A4})$$

In Figs. 14 and 15 we plot the magnetization, M , and the staggered magnetization, M_{stag} , for $x=0.0625$ and $x=0.125$, respectively. M has a small value that decreases with system size, L . This indicates that nonzero magnetization is just a finite-size effect and not an indication of long-range order. Furthermore, M remains constant at all temperatures and does not increase below T_g . M_{stag} , similarly to M , decreases with increasing system size, L , and there are no features indicating ordering transition. The fairly large magnetization indicates that the finite-size effects are large, and thus the scaling corrections are expected to be large. The staggered magnetization, M_{stag} , is smaller than the magnetization, M . Relatively large magnetization can indicate formation of short-range ferromagnetic blocks. Ferromagnetic spin blocking has been observed in experimental studies of diluted dipolar Heisenberg SG systems $\text{Eu}_x\text{Sr}_{1-x}\text{S}$ ^{57,58} and $\text{Eu}_x\text{Ca}_{1-x}\text{B}_6$.⁵⁹

Appendix B: PERIODIC BOUNDARY CONDITIONS AND SELF-INTERACTION

We consider a dipolar Hamiltonian of the form

$$\mathcal{H} = \frac{1}{2} \epsilon_d \sum_{i,j,\mu,\nu} \frac{\delta^{\mu\nu} r_{ij}^2 - 3r_{ij}^\mu r_{ij}^\nu}{r_{ij}^5} S^\mu(\mathbf{r}_i) S^\nu(\mathbf{r}_j), \quad (\text{B1})$$

where μ and ν are vector components, $\mu, \nu = x, y$ or z . \mathcal{H} can be written as

$$\mathcal{H} = \frac{1}{2} \epsilon_d \sum_{i,j,\mu,\nu} \mathcal{L}_{ij}^{\mu\nu} S_i^\mu S_j^\nu, \quad (\text{B2})$$

or shorter

$$\mathcal{H} = \frac{1}{2} \epsilon_d \sum_{i,j} \mathbf{S}_i \hat{\mathcal{L}}_{ij} \mathbf{S}_j, \quad (\text{B3})$$

where

$$\mathcal{L}_{ij} = \mathcal{L}(\mathbf{r}_{ij}) = \frac{\delta_{ij} |\mathbf{r}_{ij}|^2 - 3r_{ij}^\mu r_{ij}^\nu}{|\mathbf{r}_{ij}|^5}. \quad (\text{B4})$$

To impose periodic boundary conditions, we replace the interaction matrix, \mathcal{L}_{ij} , with

$$L_{ij}^{\mu\nu} = \sum_{\mathbf{n}}' \frac{\delta_{ij} |\mathbf{r}_{ij} + \mathbf{n}|^2 - 3(\mathbf{r}_{ij} + \mathbf{n})^\mu (\mathbf{r}_{ij} + \mathbf{n})^\nu}{|\mathbf{r}_{ij} + \mathbf{n}|^5}, \quad (\text{B5})$$

where $\mathbf{n} = kL\hat{x} + lL\hat{y} + mL\hat{z}$; k, l, m are integers and \hat{x}, \hat{y} and \hat{z} are unit vectors. L is the linear dimension of the cubic simulation box in units of a , the linear size of the cubic unit cell. $\sum_{\mathbf{n}}'$ means that the summation does not include the $\mathbf{n}=0$ term for $i=j$, where $\mathbf{r}_{ij}=0$. One must be aware of the presence of the ($\mathbf{n} \neq 0$) self-interaction term

$$L_{ii}^{\mu\nu} = \sum_{\mathbf{n} \neq 0} \frac{\delta_{ij} |\mathbf{n}|^2 - 3\mathbf{n}^\mu \mathbf{n}^\nu}{|\mathbf{n}|^5}. \quad (\text{B6})$$

The self-interaction term describes the interaction of a dipole with its own periodic images replicated outside the simulation box. For a cubic simulation box it reduces to a simple form $L_{ii}^{\mu\nu} = L_{ii} \delta_{\mu\nu}$. To show that the off-diagonal terms are zero, for $\mu \neq \nu$ we write

$$L_{ii}^{\mu\nu} = -3 \sum_{\mathbf{n} \neq 0, \mathbf{n}^\mu > 0} \frac{\mathbf{n}^\mu \mathbf{n}^\nu + (-\mathbf{n}^\mu) \mathbf{n}^\nu}{|\mathbf{n}|^5} = 0. \quad (\text{B7})$$

And further, in cubic symmetry, all three directions \hat{x}, \hat{y} and \hat{z} are equivalent; hence, $L_{ii}^{xx} = L_{ii}^{yy} = L_{ii}^{zz}$.

Appendix C: EWALD SUMMATION

We wish to calculate the lattice sum

$$L_{ij}^{\mu\nu} = \sum_{\mathbf{n}}' \frac{\delta_{ij} |\mathbf{r}_{ij} + \mathbf{n}|^2 - 3(\mathbf{r}_{ij} + \mathbf{n})^\mu (\mathbf{r}_{ij} + \mathbf{n})^\nu}{|\mathbf{r}_{ij} + \mathbf{n}|^5}. \quad (\text{C1})$$

Again, the prime symbol in the summation sign means that for $i = j$ the sum does not include the $\mathbf{n}=0$ term. Noting that

$$-\nabla_\mu \nabla_\nu \frac{1}{r} = \frac{\delta_{\mu\nu} r^2 - 3r_\mu r_\nu}{r^5}, \quad (\text{C2})$$

we write

$$L_{ij}^{\mu\nu} = -\nabla_\mu \nabla_\nu \sum_{\mathbf{n}}' \frac{1}{|\mathbf{r}_{ij} + \mathbf{n}|}; \quad (\text{C3})$$

hence, we may calculate the lattice summation for a Coulomb potential and obtain the sums for dipolar interactions by taking derivatives afterwards.

The infinite sum (C3) is conditionally convergent, meaning that the result depends on the asymptotic order of summation. The Coulomb or dipolar potential is slowly decaying at large distances; hence, with direct summation, it converges slowly. To alleviate these problems, the summation is performed using the method introduced by Ewald.^{77,78,79,80} In the Ewald technique, we separate the summation into two rapidly convergent sums: one performed in the direct (real) space and the other sum performed in the reciprocal space. Here we show only a simplified derivation, rigorous mathematical proofs and detailed discussions can be found in Ref. [80].

Using the relation

$$\frac{1}{r} = \frac{2}{\sqrt{\pi}} \int_0^\infty e^{-r^2 \rho^2} d\rho, \quad (\text{C4})$$

we write

$$\frac{1}{r} = \frac{2}{\sqrt{\pi}} \int_0^\alpha e^{-r^2 \rho^2} d\rho + \frac{\text{erfc}(\alpha r)}{r}, \quad (\text{C5})$$

where

$$\text{erfc}(x) = 1 - \text{erf}(x) = \frac{2}{\sqrt{\pi}} \int_x^\infty e^{-y^2} dy \quad (\text{C6})$$

is the complementary error function. The second term in Eq. (C5), for large α , is decreasing fast with increasing r ; hence, it converges rapidly in the summation over \mathbf{n} . The first term falls to zero slowly with increasing r , but it converges rapidly in a reciprocal space summation formulation. The splitting parameter α is chosen such that

both real space and reciprocal space sums are converging equivalently rapidly. To obtain the reciprocal space summation term we use the relation

$$\frac{2}{\sqrt{\pi}} \sum_{\mathbf{n}} e^{-(\mathbf{r}+\mathbf{n})^2 \rho^2} = \frac{2\pi}{L^3} \sum_{\mathbf{K}} \rho^{-3} e^{-K^2/4\rho^2} e^{i\mathbf{K}\cdot\mathbf{r}}, \quad (\text{C7})$$

where \mathbf{K} are the reciprocal lattice vectors, $\mathbf{n} = L(k\hat{x} + l\hat{y} + m\hat{z})$; k, l, m are integers and \hat{x}, \hat{y} and \hat{z} are unit vectors. Some care must be taken to account for the particular case of $r=0$ that corresponds to the self-interaction (B6). In that case, $n=0$ should be excluded from the summation (C3) and we write

$$\frac{2}{\sqrt{\pi}} \sum_{\mathbf{n} \neq 0} e^{-(\mathbf{r}+\mathbf{n})^2 \rho^2} = \frac{2\pi}{L^3} \sum_{\mathbf{K}} \rho^{-3} e^{-K^2/4\rho^2} e^{i\mathbf{K}\cdot\mathbf{r}} - \frac{2}{\sqrt{\pi}} e^{-r^2 \rho^2}. \quad (\text{C8})$$

Noting that

$$\int_0^\alpha d\rho \rho^{-3} e^{-K^2/4\rho^2} = \frac{2}{K^2} e^{-K^2/4\alpha^2}, \quad (\text{C9})$$

we can write

$$\begin{aligned} \sum_{\mathbf{n}}' \frac{1}{|\mathbf{r}_{ij} + \mathbf{n}|} &= \sum_{\mathbf{n}}' \frac{\text{erfc}(\alpha |\mathbf{r}_{ij} + \mathbf{n}|)}{|\mathbf{r}_{ij} + \mathbf{n}|} \\ &+ \sum_{\mathbf{K} \neq 0} \frac{4\pi}{L^3 K^2} e^{-K^2/4\alpha^2} e^{i\mathbf{K}\cdot\mathbf{r}_{ij}} \\ &- \frac{2\alpha}{\sqrt{\pi}} \delta_{ij}. \end{aligned} \quad (\text{C10})$$

The divergent, $\mathbf{K}=0$ term in the reciprocal lattice summation is omitted.

To calculate the dipolar sum in (C3), we need to take derivative of expression (C8). To start, we compute

$$-\nabla_\mu \nabla_\nu \frac{\text{erfc}(\alpha r)}{r} = \frac{\delta_{\mu\nu} B(r) r^2 - C(r) r_\mu r_\nu}{r^5}, \quad (\text{C11})$$

where

$$B(r) = \text{erfc}(r) + \frac{2\alpha r}{\sqrt{\pi}} e^{-\alpha^2 r^2}, \quad (\text{C12})$$

and

$$C(r) = 3\text{erfc}(r) + \frac{2\alpha r(3 + 2\alpha^2 r^2)}{\sqrt{\pi}} e^{-\alpha^2 r^2}. \quad (\text{C13})$$

For the reciprocal space part we compute

$$-\nabla_\mu \nabla_\nu e^{i\mathbf{K}\cdot\mathbf{r}} = K_\mu K_\nu e^{i\mathbf{K}\cdot\mathbf{r}}.$$

To obtain the self term (the last term in Eq. C8) we write

$$-\nabla_\mu \nabla_\nu e^{-r^2 \rho^2} = 2\rho^2 (\delta_{\mu\nu} - 2\rho^2 r_\mu r_\nu) e^{-r^2 \rho^2}, \quad (\text{C14})$$

and integrating (see Eq. C9) we get $-\frac{4\alpha^3}{3\sqrt{\pi}}\delta_{\mu\nu}\delta_{ij}$. Finally, we have

$$L_{ij}^{\mu\nu} = \sum_{\mathbf{n}}' \frac{\delta_{\mu\nu}B(r_{ij})r_{ij}^2 - C(r_{ij})r_{ij}^\mu r_{ij}^\nu}{r^5} \quad (\text{C15})$$

$$+ \frac{4\pi}{L^3} \sum_{\mathbf{K} \neq 0} \frac{K_\mu K_\nu}{K^2} e^{-K^2/4\alpha^2} e^{i\mathbf{K} \cdot \mathbf{r}_{ij}} \quad (\text{C16})$$

$$- \frac{4\alpha^3}{3\sqrt{\pi}}\delta_{\mu\nu}\delta_{ij}. \quad (\text{C17})$$

Similarly to the Coulomb case (C10), the divergent $\mathbf{K}=0$ term is omitted in the reciprocal space summation.

The effect of the magnetic polarization of the surface does not vanish in the thermodynamic limit. To model the experimental case of a spherical sample, a direct (real space) sum (C1) can be computed via summing over series of spherical shells of radius r_k , where each shell consist of all vectors \mathbf{n} such that $r_k < |\mathbf{n}| < r_{k+1}$. In the Ewald method, to obtain a result equivalent to such a summation, the surface contribution to the total energy should be included, and it is of the form⁷⁹

$$U^{(\text{surf})} = \frac{2\pi}{(2\epsilon' + 1)L^3} \sum_{i,j} \boldsymbol{\mu}_i \cdot \boldsymbol{\mu}_j,$$

where ϵ' is the magnetic permeability of the surrounding medium. In the case of a long cylindrical shape the surface term is zero. In our simulations we set the surface term to zero and are therefore implicitly considering a long cylindrical sample. In practice, we set $\epsilon' = \infty$, infinite magnetic permeability outside the considered system, the so-called “metallic boundary conditions”, by analogy to the physical situation with electric, as opposed to magnetic dipoles.

Appendix D: OVERRELAXATION

It has been reported that supplementing canonical Metropolis spin updates with computationally inexpensive “overrelaxation” steps of zero energy change can substantially reduce autocorrelation times.^{86,87} Unfortunately, this technique does not provide much of a performance improvement in the case of long-range interactions and cannot be used when periodic boundary condition are imposed on a system characterized by dipolar interaction with non-cubic lattice symmetry.

In overrelaxation update, a new spin direction, \mathbf{S}'_i , is obtained by performing a reflection of the spin at site i , \mathbf{S}_i , around the local dipolar field vector, \mathbf{H}_i ,

$$\mathbf{S}'_i = -\mathbf{S}_i + 2 \frac{\mathbf{S}_i \cdot \mathbf{H}_i}{H_i^2} \mathbf{H}_i. \quad (\text{D1})$$

The local dipolar field is given by Eq. (5),

$$\mathbf{H}_k = \sum_{j \neq k} \hat{L}_{kj} \mathbf{S}_j, \quad (\text{D2})$$

where the tensor \hat{L}_{kj} stands for the dipolar interaction, as defined in Eq. (2). Using Eq. (D2), the finite-size Hamiltonian of Eq. (3) can be written in the form

$$\mathcal{H} = -\frac{1}{2} \sum_k \mathbf{S}_k \cdot \mathbf{H}_k - \frac{1}{2} \sum_k \mathbf{S}_k \hat{L}_{kk} \mathbf{S}_k, \quad (\text{D3})$$

where the local dipolar field, \mathbf{H}_k , does not include the self-term and the self term is written explicitly. Let us consider an overrelaxation move of spin \mathbf{S}_i . To make the effect of the spin move clear, we write the energy of a spin configuration before the spin move in the form

$$E = -\frac{1}{2} \mathbf{S}_i \cdot \mathbf{H}_i - \frac{1}{2} \sum_{k \neq i} \mathbf{S}_k \cdot \mathbf{H}_k - \frac{1}{2} \sum_k \mathbf{S}_k \hat{L}_{kk} \mathbf{S}_k \quad (\text{D4})$$

which is just Eq. (D3) rewritten with the term for spin \mathbf{S}_i excluded from the summation and written explicitly. After changing spin \mathbf{S}_i to \mathbf{S}'_i , according to Eq. (D1), we have

$$E' = -\frac{1}{2} \mathbf{S}'_i \cdot \mathbf{H}_i - \frac{1}{2} \sum_{k \neq i} \mathbf{S}_k \cdot \mathbf{H}'_k - \frac{1}{2} \sum_k \mathbf{S}'_k \hat{L}_{kk} \mathbf{S}'_k, \quad (\text{D5})$$

where \mathbf{H}'_k are updated dipolar fields; $\mathbf{H}'_i = \mathbf{H}_i$ and for $k \neq i$:

$$\mathbf{H}'_k = \mathbf{H}_k + \hat{L}_{ki}(\mathbf{S}'_i - \mathbf{S}_i). \quad (\text{D6})$$

Combined together, Eqs. (D1), (D4), (D5) and (D6) give

$$E' - E = \frac{1}{2} \left(\mathbf{S}'_i \hat{L}_{ii} \mathbf{S}'_i - \mathbf{S}_i \hat{L}_{ii} \mathbf{S}_i \right). \quad (\text{D7})$$

The energy does not change only if $\mathbf{S}'_i \hat{L}_{ii} \mathbf{S}'_i - \mathbf{S}_i \hat{L}_{ii} \mathbf{S}_i = 0$. This is the case when, for each μ, ν , $L_{ii}^{\mu\nu} = 0$, or for diagonal \hat{L}_{ii} , $L_{ii}^{\mu\nu} = L_{ii} \delta_{\mu\nu}$, (recalling $|\mathbf{S}'_i| = |\mathbf{S}_i| = 1$), which is satisfied in the case of cubic lattice symmetry (see Appendix B).

The fact that we do not use the overrelaxation method does not cause a large decrease of efficiency in our simulation. In the case of long-range interaction, the reflection (D1) would have to be followed by the recalculation of dipolar field, \mathbf{H}'_k , of Eq. (D6). A similar lattice sum has to be performed in the case of Metropolis updates. Most of the computation time is spent on doing such lattice sums. Hence, even if it was doable, an overrelaxation move would be practically as computationally expensive as a Metropolis update.

Appendix E: HEATBATH ALGORITHM

In the original Metropolis algorithm a random configuration update is attempted and it is accepted with a probability that depends on the change of energy following such configuration change. The updates lowering the

energy are always accepted while, if the energy is to increase, the acceptance probability is

$$P(\Delta E) = \exp(-\beta \Delta E), \quad (\text{E1})$$

where $\beta = 1/k_B T$. The probability exponentially decreases with an increase of the energy change, ΔE . Thus, to obtain a sufficient acceptance rate, the attempted moves have to be sufficiently small. Usually the configuration update is chosen in such way that the acceptance rate is close to 50%. In many applications a better way of performing a local spin updates is the “heatbath” algorithm,^{88,89,90} where the new direction of a spin is drawn from a suitable probability distribution such that the new configuration energy is distributed according to a Boltzmann weight. In the case of isotropic (O(3)) Heisenberg model, the distribution of angle θ between the local dipolar field, \mathbf{H}_i , and the spin vector \mathbf{S}_i can be calculated analytically.^{88,89,90} In such an isotropic case, the Hamiltonian can be written as

$$\mathcal{H} = -\frac{1}{2} \sum_i \mathbf{S}_i \cdot \mathbf{H}_i \quad (\text{E2})$$

where \mathbf{H}_i is the interaction field and \mathbf{H}_i does not depend on spin \mathbf{S}_i . We did not include here the self-interaction term because the calculation shown below is not possible with a general self-interaction term included. The case of diagonal self-interaction term, as in the case of cubic symmetry, will be discussed at the end of this appendix. In the case of long-range interaction we write

$$\mathbf{H}_i = \sum_{j \neq i} \hat{L}_{ij} \mathbf{S}_j \quad (\text{E3})$$

It is convenient to describe spin \mathbf{S}_i in polar coordinates, θ and ϕ , with the polar axis along the local dipolar field, \mathbf{H}_i . The energy of spin i in the field of other spins is

$$E_i = -\mathbf{S}_i \cdot \mathbf{H}_i = -H_i \cos(\theta), \quad (\text{E4})$$

where θ is the polar angle defined as the angle between \mathbf{S}_i and \mathbf{H}_i . We wish to randomly choose \mathbf{S}_i such that the probability distribution of the energy (E4) given by Boltzmann distribution. The energy does not depend on the azimuthal angle, ϕ ; hence, ϕ is randomly chosen from the uniform distribution on the interval $[0, 2\pi]$. The polar angle, θ , is chosen such that $x = \cos(\theta)$ is given by the probability distribution

$$P(x) = \frac{e^{\beta H_i x}}{\int_{-1}^1 dx e^{\beta H_i x}} = \frac{\beta H_i}{2 \sinh \beta H_i} e^{\beta H_i x}, \quad (\text{E5})$$

where $\beta = 1/T$. To obtain random variable x drawn from distribution (E5), we calculate the cumulative distribution

$$F(x) = \int_{-1}^x P(x') dx' = \frac{e^{\beta H_i x} - e^{-\beta H_i}}{e^{\beta H_i} - e^{-\beta H_i}} \quad (\text{E6})$$

and we reverse $r \equiv F(x)$, where $r \in [0, 1]$ is a uniformly distributed random number. We obtain^{88,89,90}

$$x = \frac{1}{\beta H_i} \ln [1 + r (e^{2\beta H_i} - 1)] - 1. \quad (\text{E7})$$

Having chosen ϕ and θ , we need to compute the vector components of the spin and rotate them to the global coordinate system. Using the coordinates ϕ and θ , relative to the local molecular field, \mathbf{H}_k , we compute the new spin vector, $\mathbf{S}_i = (S_x, S_y, S_z)$, as follows. Let ϕ_H and θ_H denote azimuthal and polar angle of vector \mathbf{H}_i in global coordinates. A possible choice of the local coordinates \hat{x}' , \hat{y}' and \hat{z}' , having \hat{z}' axis along \mathbf{H}_i is

$$\begin{aligned} \hat{x}' &= \cos(\theta_H) \cos(\phi_H) \hat{x} + \cos(\theta_H) \sin(\phi_H) \hat{y} - \sin(\theta_H) \hat{z} \\ \hat{y}' &= -\sin(\phi_H) \hat{x} + \cos(\phi_H) \hat{y} \\ \hat{z}' &= \sin(\theta_H) \cos(\phi_H) \hat{x} + \sin(\theta_H) \sin(\phi_H) \hat{y} + \cos(\theta_H) \hat{z}. \end{aligned} \quad (\text{E8})$$

The new spin, \mathbf{S}_i , in local coordinates is

$$\mathbf{S}_i = \sin(\theta) \cos(\phi) \hat{x}' + \sin(\theta) \sin(\phi) \hat{y}' + \cos(\theta) \hat{z}', \quad (\text{E9})$$

and finally, combining Eq. (E8) and Eq. (E9), we get

$$\begin{aligned} S_x &= \Theta \cos(\phi_H) - \sin(\theta) \sin(\phi) \sin(\phi_H), \\ S_y &= \Theta \sin(\phi_H) + \sin(\theta) \sin(\phi) \cos(\phi_H), \\ S_z &= -\sin(\theta) \cos(\phi) \sin(\theta_H) + \cos(\theta) \cos(\theta_H), \end{aligned} \quad (\text{E10})$$

where

$$\Theta = \sin(\theta) \cos(\phi) \cos(\theta_H) + \cos(\theta) \sin(\theta_H). \quad (\text{E11})$$

Hamiltonian (E2) with dipolar field (E3) does not include a self-interaction term. In the case of dipolar interaction with periodic boundary condition we have to include such a self-interaction term as in the Hamiltonian of Eq. (D3). For clarity, we write this Hamiltonian again

$$\mathcal{H} = -\frac{1}{2} \sum_i (\mathbf{S}_i \mathbf{H}_i + \mathbf{S}_i \hat{L}_{ii} \mathbf{S}_i). \quad (\text{E12})$$

For Hamiltonian (E12), as opposed to Hamiltonian (E2), for a general form of the matrix \hat{L}_{ii} , the cumulative distribution (E6) cannot be integrated and reversed analytically. However, for cubic symmetry, the self-interaction term is of the form $L_{ii}^{\mu\nu} = L_{ii} \delta_{\mu\nu}$ and Eq. (E12) reduces to

$$\mathcal{H} = -\frac{1}{2} \sum_i (\mathbf{S}_i \mathbf{H}_i + L_{ii}); \quad (\text{E13})$$

hence, it is of the form (E2), with just a constant independent of spin configuration added, and the heatbath method can be applied.

Although we have cubic symmetry in our system and the heatbath algorithm could in principle be used, we decided to employ a method generally applicable for any lattice symmetry and we did not use the heatbath method.

- ¹ G. Parisi, Phys. Rev. Lett. **43**, 1754 (1979).
- ² M. Mezard, G. Parisi, and M. A. Virasoro, *Spin Glass Theory and Beyond* (World Scientific, Singapore, 1987).
- ³ D. Sherrington and S. Kirkpatrick, Phys. Rev. Lett. **35**, 1792 (1975).
- ⁴ K. H. Fischer and J. A. Hertz, *Spin Glasses* (Cambridge University Press, 1991).
- ⁵ D. S. Fisher and D. A. Huse, Phys. Rev. Lett. **56**, 1601 (1986).
- ⁶ T. Jörg, H. G. Katzgraber, and F. Krzakala, Phys. Rev. Lett. **100**, 197202 (2008).
- ⁷ S. F. Edwards and P. W. Anderson, J. Phys. F **5**, 965 (1975).
- ⁸ K. Binder and A. P. Young, Rev. Mod. Phys. **58**, 801 (1986).
- ⁹ A. T. Ogielski and I. Morgenstern, Phys. Rev. Lett. **54**, 928 (1985).
- ¹⁰ R. N. Bhatt and A. P. Young, Phys. Rev. Lett. **54**, 924 (1985).
- ¹¹ H. G. Ballesteros, A. Cruz, L. A. Fernández, V. Martín-Mayor, J. Pech, J. J. Ruiz-Lorenzo, A. Tarancón, P. Téllez, C. L. Ullod, and C. Ungil, Phys. Rev. B **62**, 14237 (2000).
- ¹² H. G. Katzgraber, M. Körner, and A. P. Young, Phys. Rev. B **73**, 224432 (2006).
- ¹³ M. Hasenbusch, A. Pelissetto, and E. Vicari, Phys. Rev. B **78**, 214205 (2008).
- ¹⁴ Ref. 13 provides a comprehensive list of references concerning numerical simulations of Ising spin glasses.
- ¹⁵ E. Marinari, G. Parisi, and F. Ritort, J. Phys. A **27**, 2687 (1994).
- ¹⁶ B. W. Morris, S. G. Colborne, M. A. Moore, A. J. Bray, and J. Canisius, J. Phys. C: Solid State Physics **19**, 1157 (1986).
- ¹⁷ M. J. P. Gingras, Phys. Rev. Lett. **71**, 1637 (1993). See references therein.
- ¹⁸ H. Kawamura, J. Magn. Magn. Mater. **310**, 1487 (2007).
- ¹⁹ H. Kawamura, Phys. Rev. Lett. **68**, 3785 (1992).
- ²⁰ H. Kawamura, Phys. Rev. Lett. **80**, 5421 (1998).
- ²¹ K. Hukushima and H. Kawamura, Phys. Rev. B **72**, 144416 (2005).
- ²² I. Campos, M. Cotallo-Aban, V. Martin-Mayor, S. Perez-Gaviro, and A. Tarancón, Phys. Rev. Lett. **97**, 217204 (2006).
- ²³ L. W. Lee and A. P. Young, Phys. Rev. B **76**, 024405 (2007).
- ²⁴ D. X. Viet and H. Kawamura, Phys. Rev. Lett. **102**, 027202 (2009).
- ²⁵ D. X. Viet and H. Kawamura, Phys. Rev. B **80**, 064418 (2009).
- ²⁶ L. A. Fernandez, V. Martin-Mayor, S. Perez-Gaviro, A. Tarancón, and A. P. Young, Phys. Rev. B **80**, 024422 (2009).
- ²⁷ M. Weigel and M. J. P. Gingras, Phys. Rev. Lett. **96**, 097206 (2006).
- ²⁸ M. Weigel and M. J. P. Gingras, Phys. Rev. B **77**, 104437 (2008).
- ²⁹ M. Weigel and M. J. P. Gingras, J. Phys.: Condensed Matter **19**, 145217 (2007).
- ³⁰ A. Ito, H. Aruga, E. Torikai, M. Kikuchi, Y. Syono, and H. Takei, Phys. Rev. Lett. **57**, 483 (1986).
- ³¹ K. Gunnarsson, P. Svedlindh, P. Nordblad, L. Lundgren, H. Aruga, and A. Ito, Phys. Rev. B **43**, 8199 (1991).
- ³² S. Nair and A. K. Nigam, Phys. Rev. B **75**, 214415 (2007).
- ³³ I. S. Suzuki and M. Suzuki, Phys. Rev. B **68**, 094424 (2003).
- ³⁴ I. S. Suzuki and M. Suzuki, Phys. Rev. B **78**, 214404 (2008).
- ³⁵ H. Maletta and W. Felsch, Phys. Rev. B **20**, 1245 (1979).
- ³⁶ H. G. Bohn, W. Zinn, B. Dorner, and A. Kollmar, Phys. Rev. B **22**, 5447 (1980).
- ³⁷ However, the case of dense amorphous systems with Ising spins can remain ferromagnetic [38,39].
- ³⁸ G. Ayton, M. J. P. Gingras, and G. N. Patey, Phys. Rev. Lett. **75**, 2360 (1995).
- ³⁹ G. Ayton, M. J. P. Gingras, and G. N. Patey, Phys. Rev. E **56**, 562 (1997).
- ⁴⁰ W. Luo, S. R. Nagel, T. F. Rosenbaum, and R. E. Rosensweig, Phys. Rev. Lett. **67**, 2721 (1991).
- ⁴¹ J. F. Fernández, Phys. Rev. B **78**, 064404 (2008).
- ⁴² J. F. Fernández and J. J. Alonso, Phys. Rev. B **79**, 214424 (2009).
- ⁴³ D. H. Reich, B. Ellman, J. Yang, T. F. Rosenbaum, G. Aeppli, and D. P. Belanger, Phys. Rev. B **42**, 4631 (1990).
- ⁴⁴ C. Ancona-Torres, D. M. Silevitch, G. Aeppli, and T. F. Rosenbaum, Phys. Rev. Lett. **101**, 057201 (2008).
- ⁴⁵ J. A. Quilliam, S. Meng, C. G. A. Mugford, and J. B. Kycia, Phys. Rev. Lett. **101**, 187204 (2008).
- ⁴⁶ K.-M. Tam and M. J. P. Gingras, Phys. Rev. Lett. **103**, 087202 (2009).
- ⁴⁷ S. Ghosh, T. F. Rosenbaum, G. Aeppli, and S. N. Coppersmith, Nature **425**, 48 (2003).
- ⁴⁸ D. H. Reich, T. F. Rosenbaum, and G. Aeppli, Phys. Rev. Lett. **59**, 1969 (1987).
- ⁴⁹ P. E. Jönsson, R. Mathieu, W. Wernsdorfer, A. M. Tkachuk, and B. Barbara, Phys. Rev. Lett. **98**, 256403 (2007).
- ⁵⁰ P. E. Jönsson, R. Mathieu, W. Wernsdorfer, A. M. Tkachuk, and B. Barbara, cond-mat/0803.1357 (2008).
- ⁵¹ J. Snider and C. C. Yu, Phys. Rev. B **72**, 214203 (2005).
- ⁵² A. Biltmo and P. Henelius, Phys. Rev. B **78**, 054437 (2008).
- ⁵³ J. J. Alonso and J. F. Fernández, arXiv:0912.1773.
- ⁵⁴ A. J. Bray and M. A. Moore, J. Phys. C **15**, 3897 (1982).
- ⁵⁵ A. J. Bray, M. A. Moore, and A. P. Young, Phys. Rev. Lett. **56**, 2641 (1986).
- ⁵⁶ N. W. Dalton, C. Domb, and M. F. Sykes, Proceedings of the Physical Society **83**, 496 (1964).
- ⁵⁷ J. L. Tholence, J. App. Phys. **50**, 7369 (1979).
- ⁵⁸ J. Kötzler and G. Eiselt, Phys. Rev. B **25**, 3207 (1982).
- ⁵⁹ G. Wigger, E. Felder, M. Weller, S. Streule, H. Ott, A. Bianchi, and Z. Fisk, Eur. Phys. J. B **46**, 231 (2005).
- ⁶⁰ N. P. Raju, M. Dion, M. J. P. Gingras, T. E. Mason, and J. E. Greedan, Phys. Rev. B **59**, 14489 (1999).
- ⁶¹ V. Bondah-Jagalu and S. T. Bramwell, Can. J. Phys. **79**, 1381 (2001).
- ⁶² J. S. Gardner, M. J. P. Gingras, and J. E. Greedan, (to appear in Rev. Mod. Phys.).
- ⁶³ P. Bonville, J. A. Hodges, M. Ocio, J. P. Sanchez, P. Vullet, S. Sosin, and D. Braithwaite, J. Phys.: Condensed Matter **15**, 7777 (2003).

- ⁶⁴ R. Moessner and J. T. Chalker, Phys. Rev. Lett. **80**, 2929 (1998).
- ⁶⁵ B. Canals and C. Lacroix, Phys. Rev. Lett. **80**, 2933 (1998).
- ⁶⁶ A. S. Wills, M. E. Zhitomirsky, B. Canals, J. P. Sanchez, P. Bonville, P. D. de Réotier, and A. Yaouanc, J. Phys.: Condens. Matter **18**, L37 (2006).
- ⁶⁷ S. E. Palmer and J. T. Chalker, Phys. Rev. B **62**, 488 (2000).
- ⁶⁸ J. D. M. Champion, A. S. Wills, T. Fennell, S. T. Bramwell, J. S. Gardner, and M. A. Green, Phys. Rev. B **64**, 140407 (2001).
- ⁶⁹ J. R. Stewart, G. Ehlers, A. S. Wills, S. T. Bramwell, and J. S. Gardner, J. Phys.: Condens. Matter **16**, L321 (2004).
- ⁷⁰ O. A. Petrenko, C. Ritter, M. Yethiraj, and D. McK Paul, Phys. Rev. Lett. **80**, 4570 (1998).
- ⁷¹ S. R. Dunsiger, J. S. Gardner, J. A. Chakhalian, A. L. Cornelius, M. Jaime, R. F. Kiefl, R. Movshovich, W. A. MacFarlane, R. I. Miller, J. E. Sonier, et al., Phys. Rev. Lett. **85**, 3504 (2000).
- ⁷² S. Ghosh, T. F. Rosenbaum, and G. Aeppli, Phys. Rev. Lett. **101**, 157205 (2008).
- ⁷³ P. Schiffer, A. P. Ramirez, D. A. Huse, P. L. Gammel, U. Yaron, D. J. Bishop, and A. J. Valentino, Phys. Rev. Lett. **74**, 2379 (1995).
- ⁷⁴ T. Yavors'kii, M. Enjalran, and M. J. P. Gingras, Phys. Rev. Lett. **97**, 267203 (2006).
- ⁷⁵ T. Yavors'kii, M. J. P. Gingras, and M. Enjalran, J. Phys.: Condens. Matter **19**, 145274 (2007).
- ⁷⁶ We also ignore weak Gd^{3+} single-ion anisotropy that would differ between materials.
- ⁷⁷ P. Ewald, Ann. Phys. **64**, 253 (1921).
- ⁷⁸ M. T. Dove, *Introduction to Lattice Dynamics* (Cambridge University Press, 1993).
- ⁷⁹ Z. Wang and C. Holm, J. Chem. Phys. **115**, 6351 (2001).
- ⁸⁰ S. W. De Leeuw, J. W. Perram, and E. R. Smith, Proc. R. Soc. London **A 373**, 27 (1980).
- ⁸¹ E. Marinari and G. Parisi, Europhys. Lett. **19**, 451 (1992).
- ⁸² K. Hukushima and K. Nemoto, J. Phys. Soc. Jpn **65**, 1604 (1996).
- ⁸³ M. H. Quenouille, Biometrika **43**, 353 (1956).
- ⁸⁴ J. W. Tukey, Ann. Math. Statist. **29**, 614 (1958).
- ⁸⁵ B. A. Berg, *Markov chain Monte Carlo simulations and their statistical analysis* (World Scientific, Singapore, 2004).
- ⁸⁶ M. Creutz, Phys. Rev. D **36**, 515 (1987).
- ⁸⁷ J. L. Alonso, A. Tarancón, H. G. Ballesteros, L. A. Fernández, V. Martín-Mayor, and A. Muñoz Sudupe, Phys. Rev. B **53**, 2537 (1996).
- ⁸⁸ M. Creutz, Phys. Rev. D **21**, 2308 (1980).
- ⁸⁹ Y. Miyatake, M. Yamamoto, J. J. Kim, M. Toyonaga, and O. Nagai, J. Phys. C **19**, 2539 (1986).
- ⁹⁰ J. A. Olive, A. P. Young, and D. Sherrington, Phys. Rev. B **34**, 6341 (1986).
- ⁹¹ K. Binder, Z. Phys. B **43**, 119 (1981).
- ⁹² D. P. Landau and K. Binder, *A Guide to Monte Carlo Simulations in Statistical Physics* (Cambridge University Press, 2000).
- ⁹³ K. Binder, Phys. Rev. Lett. **47**, 693 (1981).
- ⁹⁴ We do not call the function \tilde{X} universal because it implicitly contains a non-universal factor, as opposite to the case when a scaling formula is written as $U_L = \tilde{X}'(AL^{1/\nu}(T - T_g))$, with a non-universal constant, A , given explicitly and \tilde{X}' being a universal scaling function.^{12,95}
- ⁹⁵ V. Privman and M. E. Fisher, Phys. Rev. B **30**, 322 (1984).
- ⁹⁶ A. D. Beath and D. H. Ryan, J. Appl. Phys. **97**, 10A506 (2005).
- ⁹⁷ In the case of parallel tempering simulations the data are always smooth due to the correlations between the thermal replicas.
- ⁹⁸ F. Schwabl, *Statistical mechanics* (Springer, Berlin Heidelberg New York, 2006).
- ⁹⁹ F. Cooper, B. Freedman, and D. Preston, Nucl. Phys. B **210**, 210 (1982).
- ¹⁰⁰ J. M. Luttinger and L. Tisza, Phys. Rev. **70**, 954 (1946).
- ¹⁰¹ S. Romano, IL Nuovo Cimento **7**, 717 (1986).
- ¹⁰² T. Jörg, Phys. Rev. B **73**, 224431 (2006).
- ¹⁰³ F. Matsubara, T. Shirakura, S. Endoh, and S. Takahashi, Journal of Physics A: Mathematical and General **36**, 10881 (2003).
- ¹⁰⁴ T. Shirakura and F. Matsubara, Phys. Rev. B **67**, 100405 (2003).
- ¹⁰⁵ I. A. Campbell, K. Hukushima, and H. Takayama, Phys. Rev. Lett. **97**, 117202 (2006).
- ¹⁰⁶ J. F. Fernández and J. J. Alonso, Phys. Rev. B **73**, 024412 (2006).